P. SHARIEF*, B. MADAVALI*, J.M. KOO*#, H.J. KIM**, S. HONG***, S.-J. HONG*#

EFFECT OF MILLING TIME PARAMETER ON THE MICROSTRUCTURE AND THE THERMOELECTRIC PROPERTIES OF N-TYPE $Bi_2Te_{2.7}Se_{0.3}$ ALLOYS

Nanostructured thermoelectric materials receiving great attention for its high thermoelectric performance. In this research, nanostructured n-type $Bi_2Te_{2.7}Se_{0.3}$ alloys have prepared using high energy ball milling and followed by spark plasma sintering. Also, we have varied ball milling time to investigate milling time parameter on the thermoelectric properties of n-type $Bi_2Te_{2.7}Se_{0.3}$ powder. The powders were discrete at 10 min milling and later particles tend to agglomerate at higher milling time due to cold welding. The bulk fracture surface display multi-scale grains where small grains intersperse in between large grains. The maximum Seebeck coefficient value was obtained at 20-min milling time due to their lower carrier density. The κ values were decreased with increasing milling time due to the decreasing trend observed in their κ_L values. The highest ZT of 0.7 at 350 K was observed for 30-min milling time which was ascribed to its lower thermal conductivity. The Vickers hardness values also greatly improved due to their fine microstructure.

Keywords: Ball milling, Milling time, Microstructure, Thermoelectric properties, ZT

1. Introduction

Thermoelectric (TE) devices possesses great attention in clean and renewable energy conversion technique due to its capacity in converting waste heat energy from various sources into electrical energy and to enable electrical energy into solid state cooling to replace vapor compression refrigeration [1]. There is also a worldwide agreement to eliminate ozone depleting gases like hydro chlorofluorocarbons produced from refrigerators by 2030, creating importance for TE devices [2]. For extensive applications of TE devices and to enhance the energy conversion efficiency, high performance thermoelectric materials was a prerequisite factor. The performance of TE materials was gauged by dimensionless figure of merit, $ZT = \alpha^2 T/\rho\kappa$, where α is Seebeck coefficient, ρ is the electrical resistivity, κ is total thermal conductivity (including both lattice κ_L and electronic contribution κ_e) and T is the absolute temperature respectively. There is a trade-off relationship in between α, ρ, and κ making quite stressful to enhance ZT [3-7]. To improve ZT, several strategies like band convergence [3], texture control [4], nanoinclusion [5], nanostructuring [6], and phonon-glass-electron-crystal principle [7] were implemented.

Among thermoelectric materials, bismuth telluride (Bi_2Te_3) based alloys were the best candidate for thermoelectric cooling applications and low temperature power generation due to its high ZT value at near room temperature and currently, these materials were widely used in commercial applications [3,8]. One of the key strategies to improve the ZT value of bismuth telluride alloy was to reduce 'κ' value and it has proven that nanostructuring was an efficient method in drastically reducing thermal conductivity resulting high ZT [9, 10]. Nanostructured Bi_2Te_3 was prepared through various processing techniques which includes solvothermal method [11], water based chemical reduction [12], wet chemical method [13], refluxing [14], polyol [15], and arc melting [16]. Yang et al. [11] produced Bi_2Te_3 nanostructured material through solvothermal method and sintering through spark plasma technique. The consolidated sample shows an ultralow lattice thermal conductivity of 0.2 W/m-K which comes from high-density small-angle grain boundaries embedded by dislocations resulting ZT of 0.88 at 400 K. Gharshallah et al. [16] prepared nanosized Bi_2Te_3 material using arc melting method and the bulk displays many surface boundaries which improves phonon scattering factors. Saleemi et al. [17] had prepared nanostructured Bi_2Te_3 using chemical synthetic route and obtained high ZT of 1.1 at 340 K. Nevertheless, the above-mentioned methods were cost-effective and time-consuming methods which were inadequate for industrial scalable amount of nanosized thermoelectric material.

To achieve nanostructured materials combining high production rate, the powder metallurgy technique, ball-milling was considered as a feasible method. Ball milling is an effective top-down solid-state powder processing technique which produces

* KONGJU NATIONAL UNIVERSITY, DIVISION OF ADVANCED MATERIALS ENGINEERING, 1223-2, SEOBUK-GU, CHEONAN-SI, CHUNGNAM, 331-717, SOUTH KOREA
** KONGJU NATIONAL UNIVERSITY, DIVISION OF CERAMIC DESIGN, GONGJU-SI, SOUTH KOREA
*** KONGJU NATIONAL UNIVERSITY, DIVISION OF MECHANICAL AND AUTOMOTIVE ENGINEERING, CHEONAN, SOUTH KOREA

Corresponding authors: hongsj@kongju.ac.kr, koo5257@kongju.ac.kr

large quantities of nanosized fine particles with in limited time, which was developed in 1970's for industrial sector [18,19]. Since 1950's, many consistent efforts had done to improve ZT above 1 for Bi_2Te_3 and its alloys for large-scale energy conversion applications. In 2008, Poudel et al. [19] had produced nano-sized p-type bismuth antimony telluride (BiSbTe) powder using ball milling technique and achieved high ZT of 1.4 at 373 K, which was a breakthrough achieved from ball milling method. Ma et al. [20] also attained ZT of 1.3 around 348 K to 373 K in BiSbTe alloy by ball milling procedure. Powder metallurgy technique, gas atomization (GA) attains high productive rate of 1-3 kg/min. Recently, Babu et al. [21] had improved the gas atomization powder ZT from 1 to 1.15 by reducing κ value through GA powder size reduction via ball milling process. Thermoelectric module which acts as thermoelectric generator and coolers, requires combination of p-type and n-type materials for small-size commercial applications. Even though, nanostructured P-type Bi_2Te_3 attained much progress and obtained considerable ZT, however n-type materials yet to be developed. Compared to P-type material, nanostructured n-type material shows low ZT [22] which impedes fabrication of thermoelectric module. Therefore, much research needed in developing n-type ZT value through ball milling route.

Therefore, in this research we used water atomized (WA) n-type $Bi_2T_{2.7}Se_{0.3}$ powder as a starting material. The nanostructured n-type $Bi_2Te_{2.7}Se_{0.3}$ powders were fabricated by using WA powders through the high energy ball milling at different milling times. Effect of various milling time on the thermoelectric properties of n-type $Bi_2Te_{2.7}Se_{0.3}$ alloys was successfully interpreted by microstructure, carrier concentration and mobility respectively.

2. Experimental procedure

The water atomized $Bi_2Te_{2.7}Se_{0.3}$ powder (<200 µm) was used as a starting powder, and ball milled at 10, 20 and 30 min respectively using high energy ball milling with 15:1 ball to powder ratio at 1100 rpm speed. The ball milled powder were consolidated with spark plasma sintering technique at 673 K holding for 10 min under 50 MPa. The phase identification of powder and bulk samples was investigated using X-ray diffraction (Rigaku, MiniFlex-600) with Cu Kα radiation. The morphology of the powder and bulk fracture microstructure was observed with scanning electron microscope (SEM-MIRA-LMH II (TESKAN)). Seebeck coefficient (α) and electrical conductivity (σ) were simultaneously measured with rectangular shaped sample within range of 300-500 K using thermoelectric measurement system (TEP-1000, Seepel). Thermal conductivity (κ) of the samples was calculated using the formula $\kappa = \lambda C_p D$, where thermal diffusivity (λ) and specific heat (C_p) was determined using laser flash method (Netzsch LFA 457 system). Density (D) was measured using Archimedes principle. The ZT values were calculated from power factor ($\alpha^2\sigma$) and κ values respectively. The carrier concentration and mobility were calculated

at room temperature using Hall measurement system (Ecopia HMS-3000). The Vickers hardness was measured using micro Vickers hardness tester.

3. Results and discussion

Fig. 1 shows the XRD phase analysis of n-type $Bi_2Te_{2.7}Se_{0.3}$ ball milled powder and their spark plasma sintered (SPS) bulk samples at different milling time. The diffraction patterns of both powders as well as bulk samples were well-matched with standard diffraction peaks (JCPDS no. #500954). The powders and their respective bulk samples were identified as Bi_2Te_3 single phase with rhombohedral crystal structure ($R\bar{3}m$ space group) and no other impurity phases were observed.
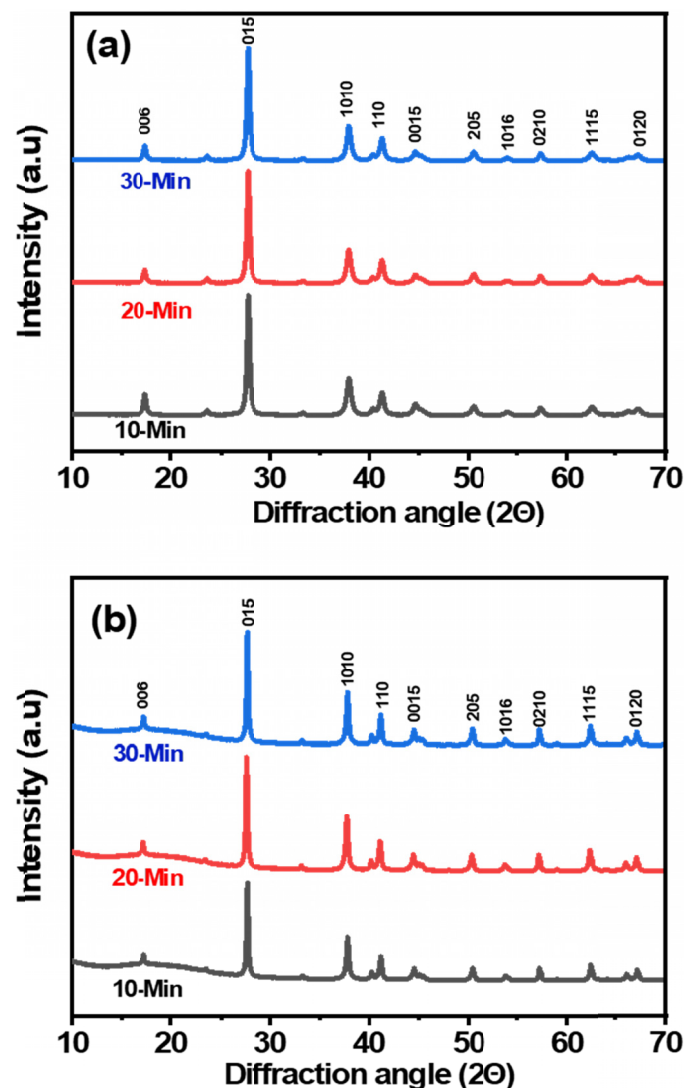

Fig. 1. X-ray diffraction analysis of (a) ball milled powder and, (b) bulk samples at various milling time

Fig. 2 displays the scanning electron microscope (SEM) images of n-type $Bi_2Te_{2.7}Se_{0.3}$ ball milled powder at different milling times. All milled powders had irregular in shape and shows wide range in size. The milled powders had displayed dis-

tinct nature in morphology. It is revealed from the Fig. 2(a) that 10-min milled powder particles were isolated with one another, while 20-min and 30-min milled powders were agglomerated with each other and forms cluster-type particle. It is evident from Fig. 2(b) that many fine particles were combined together and formed agglomeration. Ball milling process involves repeatedly flattening, cold welding, fracturing and rewelding of particles inside milling jar [18]. Hence considering 10-min milling time,
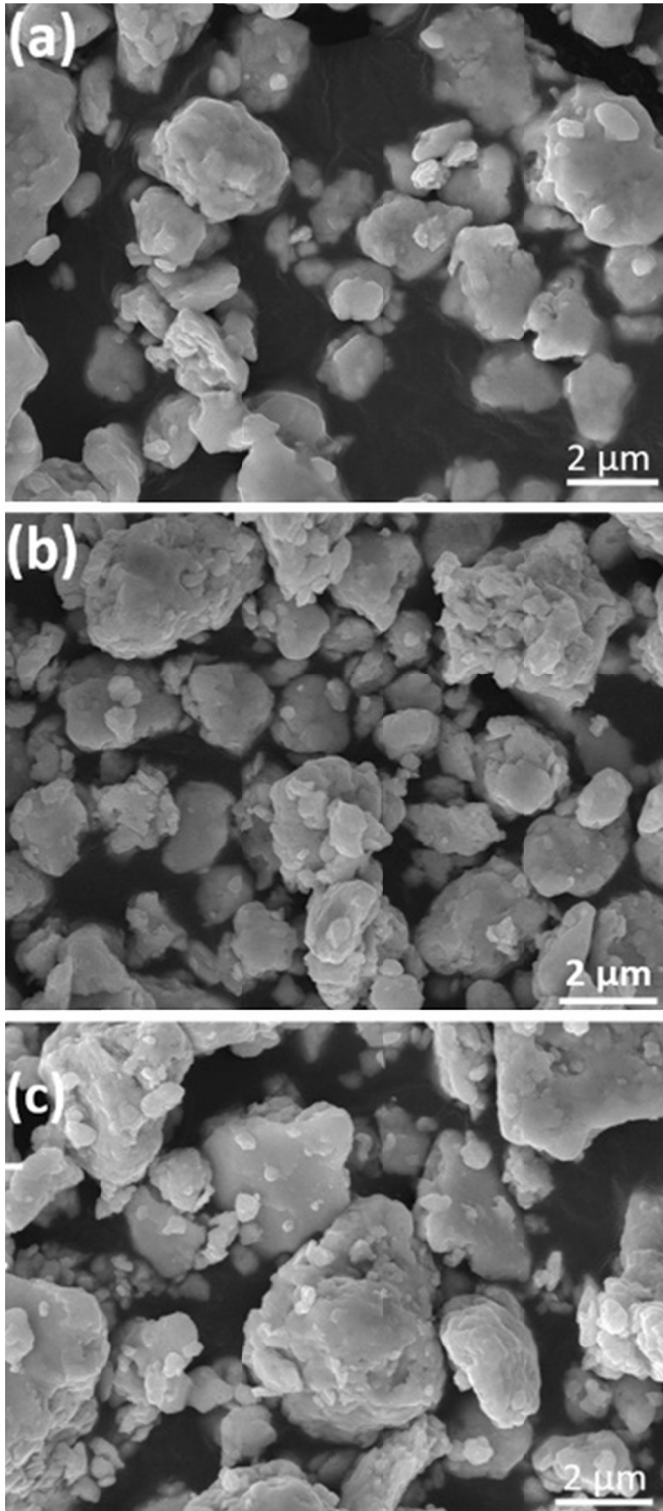
the particles were fractured and then these fractured particles were cold welded and forms cluster-type particles for longer milling times. The cold welding had enhanced with milling time; therefore, the lump shaped particles were observed in 30-min powder.

Fig. 3 shows the SEM fracture surface images of n-type $Bi_2Te_{2.7}Se_{0.3}$ ball milled bulk samples. It can be found that the

Fig. 2. SEM powder morphology images of ball milled powder at different timings, (a) 10-min, (b) 20-min, and (c) 30-min respectively
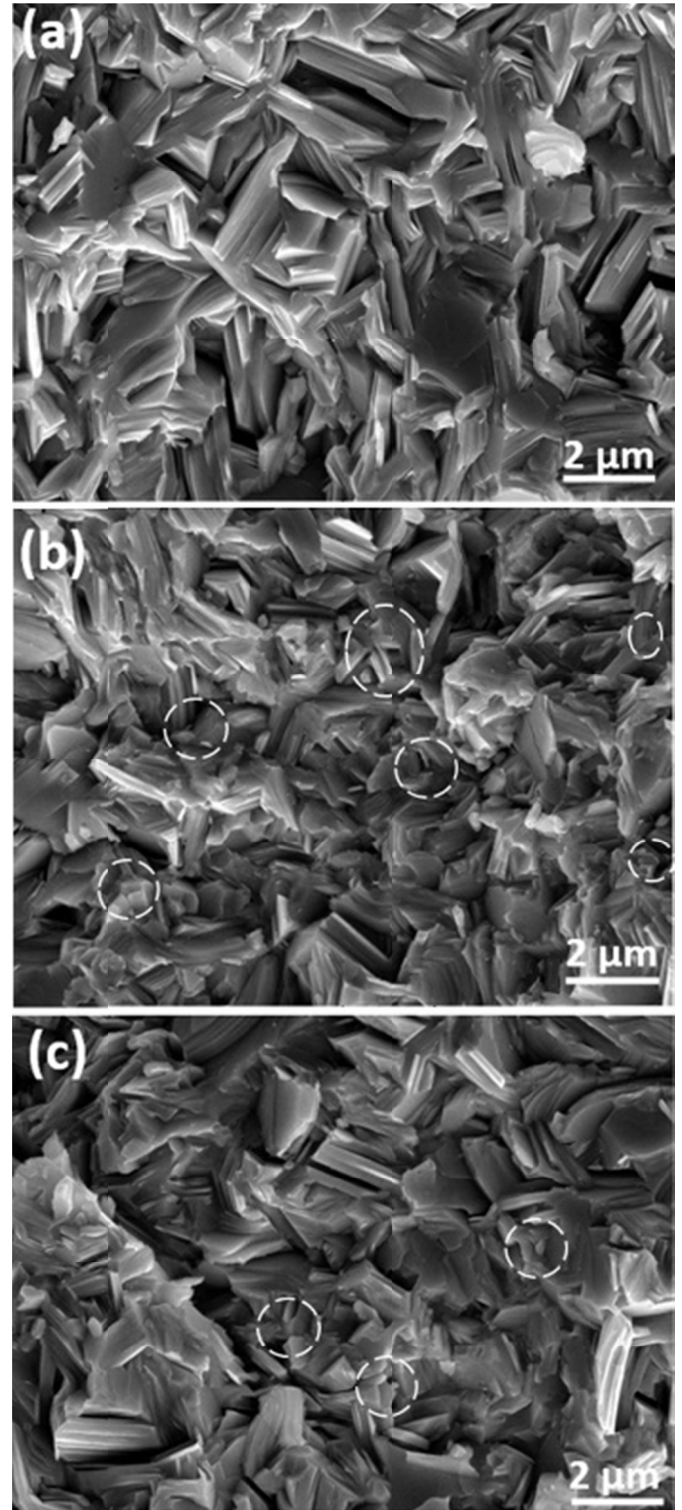

Fig. 3. SEM fracture surface images of ball milled bulk at (a) 10-min, (b) 20-min, and (c) 30- min respectively. The white dotted circle in Fig. 2(b, c) shows a fine grains distribution

granular structured grains were densely packed and randomly distributed without any preferred orientation. All the bulk samples had shown relative density of ~99% and obviously no pores were observed. As seen in Fig. 3(a), the 10-min bulk sample displays clear image with grains having similar in size, roughly about 2.5 μm. While the 20, 30 min bulk samples (see Fig. 3(b, c)) shows typical microstructure contains small size grains (shown as white dotted circles) about 0.5 μm range intersperse between
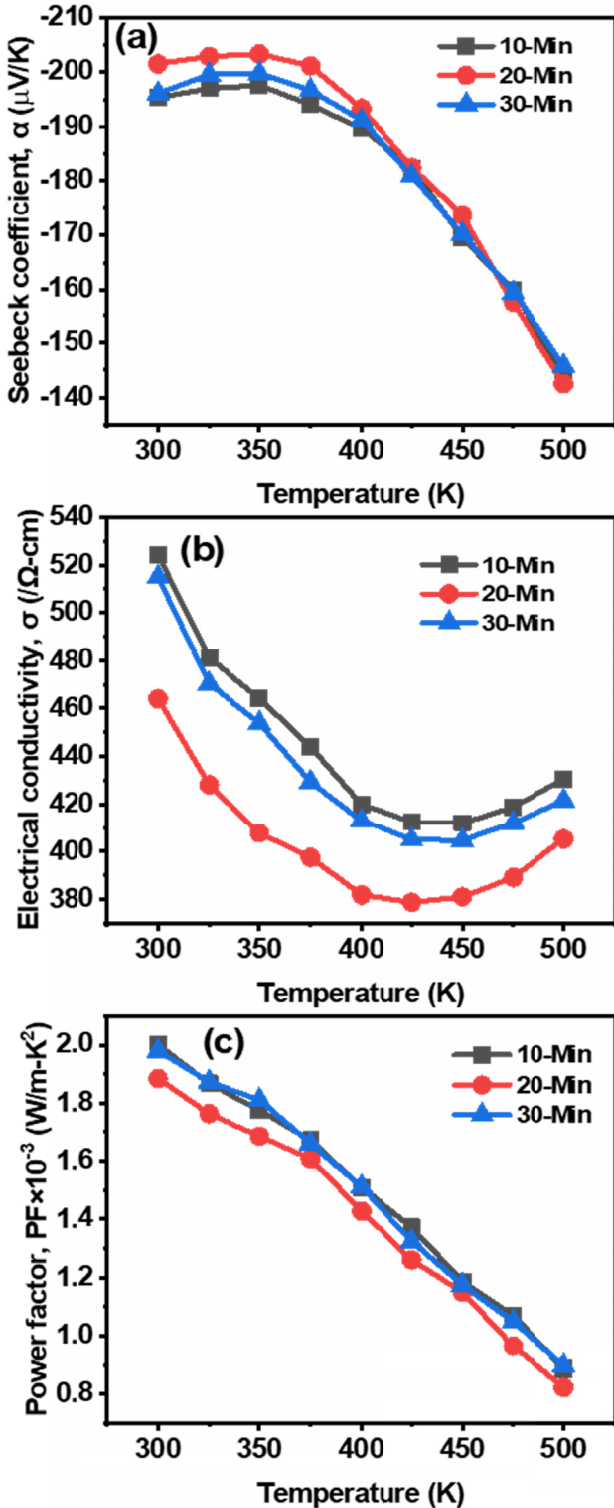
large grains and the intersperse of small grains was largely found in 20-min sample. Possibly, the formation of such typical microstructure was correlated to the powder morphology. Such kind of formation of typical microstructure can eminently affected the Seebeck coefficient, and thermal conductivity.

Fig. 4 illustrates the temperature dependence of Seebeck coefficient (α), electrical conductivity (σ) and power factor ($\alpha^2\sigma$) values for n-type $Bi_2Te_{2.7}Se_{0.3}$ SPS bulks. The Seebeck coefficient was shown in Fig. 4(a). All the samples showed negative values indicates that electrons were the majority carriers. The Seebeck coefficient value increases till 350 K in all samples and later tends to decrease with temperature. This was due to the excitation of minority carriers (holes) which have positive Seebeck value that might be reduced the overall 'α' value according [23] to the Eq. (1). as

$$\alpha = \frac{\alpha_n \sigma_n + \alpha_p \sigma_p}{\sigma_n + \sigma_n} \tag{1}$$

Where α_n, α_p were negative, positive Seebeck coefficient values and σ_n, σ_n were electron and hole electrical conductivities respectively. To interpret the trend of 'α' with milling time, we measured the carrier concentration and mobility at room temperature for three samples and listed out in Table 1. The Pisarenko relation [6] expressed in Eq. (2) correlates the carrier concentration (n) and Seebeck coefficient (α) as

$$\alpha = \frac{8\pi^2 k_B^2 T}{3eh^2} m^* \left(\frac{\pi}{3n}\right)^{2/3} \tag{2}$$

Where k_B is Boltzmann constant, e is carrier charge, m^* is effective mass, and n is carrier concentration respectively. As seen in Eq. (2), the carrier concentration and Seebeck coefficient were inversely proportional to each other. From the Table 1, the carrier concentration decreases from 1.83×10^{19} cm^{-3} to 1.73×10^{19} cm^{-3} and increases to 1.8×10^{19} cm^{-3} with milling time. Hence, the trend of 'α' values was consistent with 'n', observed through Pisarenko relation. The alteration of carrier concentration values was considered due to the microstructure changes and points defects which easily forms through ball milling technique [6,21].

Fig. 4. Temperature dependence of (a) Seebeck coefficient, (b) electrical conductivity, (c) power factor at various milling time

TABLE 1

Carrier concentration (n) and mobility (μ) at 300 K, Vickers hardness and relative density values for various milling time bulk samples

	10-Min	20-Min	30-Min
Carrier concentration (n*10^{19}) cm^{-3}	1.83	1.73	1.80
Mobility (μ) cm^2 V^{-1}S^{-1}	180.9	172.2	177.9
Vickers hardness (HV)	122.88	123.77	128.18
Relative density (%)	99.1	98.88	99.03

The electrical conductivity (σ) of n-type $Bi_2Te_{2.7}Se_{0.3}$ milled samples was illustrated in Fig. 4(b). All samples had shown same kind of trend from 300 K to 500 K temperature. The electrical conductivity displayed metallic nature till 425 K i.e., decreasing

and after tends to increase up to 500 K indicating semi-metallic behavior [23]. It is known that the semi-metallic nature, where the excitation of minority carriers by obtaining abundant excitation energy at 425 K and contributed in increasing electrical conductivity at higher temperatures [23]. At all respective temperatures, the 10-min and 30-min milled specimens obtained same 'σ' values, while 20-min bulk sample shows lower value due to the simultaneous decrement in carrier concentration (n) and mobility (μ) values (see Table 1). Fig. 4(c) shows the power factor values for all n-type $Bi_2Te_{2.7}Se_{0.3}$ specimens. All the samples had reached almost same values about 2×10^{-3} W/m-K^2 at room temperature. Despite having high Seebeck values compared to other samples, a slight reduction in power factor has been noted in 20-min sample due to its low electrical conductivity value.

Fig. 5 displays the temperature dependence of thermal conductivity and its transport properties for n-type $Bi_2Te_{2.7}Se_{0.3}$ samples. The total thermal conductivity (κ) values were illustrated in Fig. 5(a). In all samples, the κ slightly decreases to 350 K and later abruptly increases. The thermal energy transportation in materials was carried out by lattice vibrations (phonons) and charge carriers. Hence, the total thermal conductivity (κ) was a combination of electronic thermal conductivity (κ_e) and lattice thermal conductivity (κ_L) i.e., $\kappa = \kappa_e + \kappa_L$. The electronic thermal contribution can be calculated using Wiedemann-Franz law, $\kappa_e = \sigma LT$, where L is the Lorenz number equals to 2.4×10^{-8} WΩK^{-2} which perfectly fits for metals [6-8]. For semiconductor materials, the standard L value varied according to composition and it had to calculate for measuring precise κ_e value. The 'L' values can be estimated according to the Eq. (3) proposed by Kim at al. [24] and the equation as follows

$$L = 1.5 + \exp\left[-\frac{|\alpha|}{116}\right] \qquad (3)$$

We have calculated the temperature dependence of electronic thermal conductivity by estimating the 'L' values using Eq. 3 and showed in Fig. 5(b). The electronic thermal conductivity increases with temperature and the variation of κ_e values among different milling time was consistent with carrier concentration. The 10-min sample contains highest κ_e value due to its high 'n' value. The temperature dependence of lattice thermal conductivity was calculated by subtracting κ_e value from κ ($\kappa_L = \kappa - \kappa_e$) and showed in Fig. 5(c). The κ_L values were reduces with increasing milling time was plausibly due to the formation of fine grains. The κ_L value slightly decreases to 350 K and later inflected to higher values with temperature in all bulks. If minority carriers were not activated with temperature, the relation between κ_L and reciprocal of temperature ($1/T$) is theoretically linear [25]. The κ_L had to decrease with temperature but, in deed, the κ_L leads to high value with temperature which is ascribed to the subscription of minority carrier (bipolar effect) to κ_L value [15-20].

Fig. 6 shows the variation of dimensionless figure of merit (ZT) with temperature for n-type $Bi_2Te_{2.7}Se_{0.3}$ samples. Among all samples, the 30-min had improved its ZT from its neighbor samples. It was ascribed for its high-power factor and reasonable
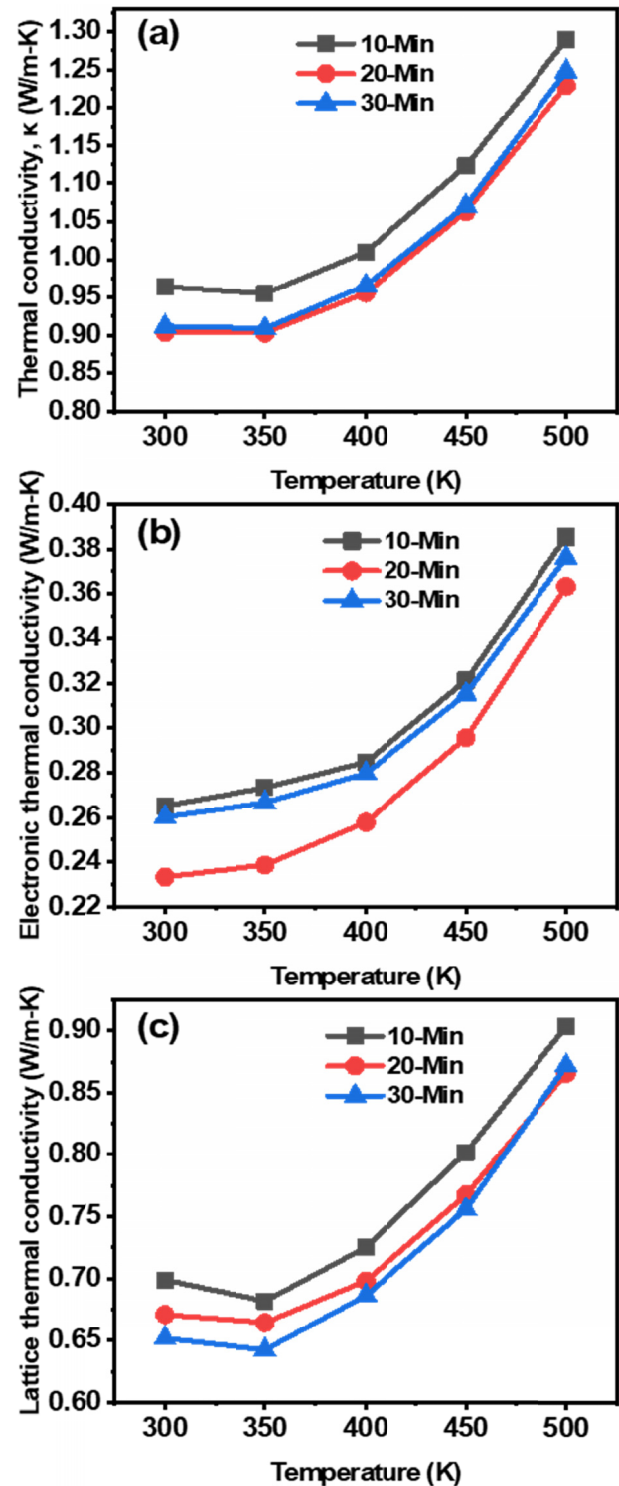

Fig. 5. Temperature dependence of (a) total thermal conductivity (κ), (b) electrical thermal conductivity (κ_e), and (c) lattice thermal conductivity (κ_L) at different milling time

low thermal conductivity contributed for enhancing ZT. Thermoelectric materials having high mechanical properties was also crucial in minimizing scrap leads to reducing TE device cost. We measured the Vickers hardness values and shown in Table 1. All samples shows hardness above 120 HV which was greatly improved than Zhao et al. [26] and Babu et al. [18] works and prevents the wastage during module fabrication.
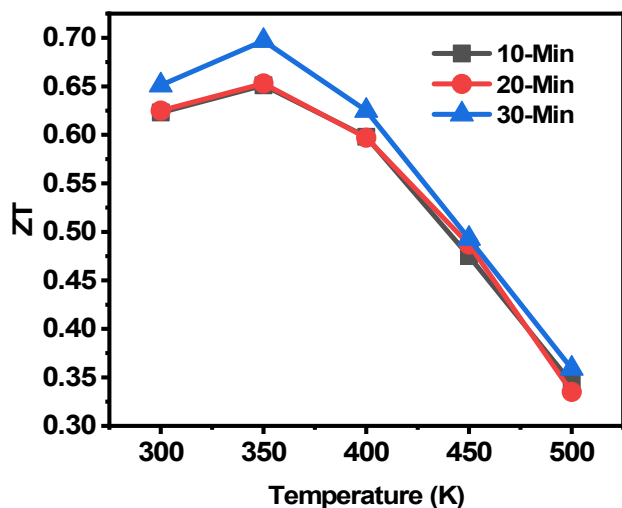
Fig. 6. Temperature dependence of figure of merit (*ZT*) for various milling time bulk samples

4. Conclusion

The nanostructured n-type $Bi_2Te_{2.7}Se_{0.3}$ alloy was successfully fabricated by high energy ball milling technique and subsequently consolidated using SPS technique. In addition, the effect of milling time (10, 20, and 30 min) on the powder morphology, microstructure and thermoelectric properties of n-type $Bi_2Te_{2.7}Se_{0.3}$ alloy was systematically studied. From phase structure analysis, it was confirmed that all powder and bulk samples had displayed singular Bi_2Te_3 phase. At 10 min, the particle was fractured and displays as unglued particles, while in 20 and 30-min powder particles were agglomerated by cold welding method. The SEM bulk fracture displays random distribution of grains and at higher milling time, fine grains were spotted in between large grains. The electronic transport properties showed its trend accordingly with microstructure and maximum electrical conductivity of 530 $\Omega^{-1}cm^{-1}$ obtained at 10-min. The thermal conductivity tends to decrease with milling time due to their low lattice thermal conductivity. Maintaining high power factor and low κ value, 30-min sample achieved high *ZT* of 0.7 at 350 K.

REFERENCES

[1] F.J. Disalvo, Science **285**, 703-706 (1999).

[2] G.J.M. Velders, A.R. Ravishankara, M.K. Miller, M.J. Molina, J. Alcamo, J.S. Daniel, D.W. Fahey, S.A. Montza, S. Reimann, SCIENCE **335**, 922-923 (2012).

[3] H.S. Kim, N.A. Heinz, Z.M. Gibbs, Y. Tang, S.D. Kang, G.F. Snyder, Mater. Today **20**, 452-458 (2017).

[4] L. Hu, Y. Zhang, H. Wu, Y. Liu, J. Li, J. He, W. Ao, F. Liu, S. Pennycook, X. Zeng, Adv. Funct. Mater. 1803617, 1-13 (2018).

[5] B. Madavali, H.S. Kim, K.H. Lee, S.J. Hong, J. Appl. Phys. **121**, 225104 (2017).

[6] Z.G. Chan, G. Han, L. Yang, L. Cheng, J. Zou, Prog. Nat. Sci. **22**, 535-549 (2016).

[7] J. Zhang, B. Xu, L. Min, D. Yu, J. Yang, F. Yu, Z. Liu, J. He, B. Wen, Y. Tian, Acta Mater. **60**, 1246-1251 (2012).

[8] Ch. Gayner, K.K. Kar, Prog. Mater Sci. **83**, 330-382 (2016).

[9] M.G. Kanatzidis, Chem. Mater. **22**, 648-659 (2010).

[10] H. Mamur, M.R.A. Bhuiyan, F. Korkmaz, M. Nil, Sust. Energ. Rev. **82**, 4159-4169 (2018).

[11] L. Yang, Z.G. Chen, M. Hong, G. Han, J. Zou, ACS Appl. Mater. Interfaces. **7**, 23694-23699 (2015).

[12] C. Kim, D.H. Kim, Y.S. Han, J.S. Chung, S.H. Park, H. Kim, Powder Technol. **214**, 463-468 (2011).

[13] P. Srivastava, K. Singh, J Therm Anal Calorim **110**, 523-527 (2012).

[14] S. Gupta, S. Neeleshwar, V. Kumar, Y.Y. Chen, Adv. Mater. Lett. **3**, 50-54 (2012).

[15] K.T. Kim, H.M. Lee, D.W. Kim, K.J. Kim, G.H. Ha, J. Korean Phys. Soc. **57** (4), 1037-1040 (2010).

[16] M. Gharsallah, F.S. Sanchez, J. Bermudez, N.M. Nemes, J.L. Martinez, F. Elhalouani, J.A. Alonso, Nanoscale Res. Lett. **11** (142), 1-7 (2016).

[17] M. Saleemi, M.S. Toprak, S. Li, M. Johnson, M. Muhammed J. Mater. Chem. **22**, 725-730 (2012).

[18] C. Suryanarayana, Prog. Mater Sci. **58**, 383-502 (2013).

[19] B. Poudel, Q. Hao, Y. Ma, Y. Lan, A. Minnich, B. Yu, X. Yan, D. Wang, A. Muto, D. Vashaee, X. Chen, J. Liu, M.S. Dresselhaus, G. Chen, Z. Ren, SCIENCE **320**, 634-638 (2008).

[20] Y. Ma, Q. Hao, B. Poudel, Y. Lan, B. Yu, D. Wang, G. Chen, Z. Ren, Nano Lett. **8** (8), 2580-2584 (2008).

[21] B. Madavali, H.S. Kim, K.P. Lee, Y. Isoda, F. Gascoin, S.J. Hong, Mater. Des. **112**, 485-494 (2016).

[22] Y. Pan, T. Wei, Q. Cao, J. Li, Mater. Sci. Eng. B **197**, 75-81 (2015).

[23] H. Julian Goldsmid, Introduction to Thermoelectricity, New York 2009.

[24] H.S. Kim, Z.M. Gibbs, Y. Tang, H. Wang, G.J. Synder, APL Mater. **3**, 041506 (2015).

[25] L. Hu, Y. Zhang, H. Wu, Y. Liu, J. Li, J. He, W. Ao, F. Liu, S.J. Pennycook, X. Zeng, Adv. Funct. Mater. **28**, 1803617 (2018).

[26] L. Zhao, B. Zhang, J. Li, M. Zhou, W. Liu, J. Liu, J. Alloys. Compd. **455**, 259-264 (2008).